

# Model Inspired by Nuclear Pore Complex Suggests Possible Roles for Nuclear Transport Receptors in Determining Its Structure

Dino Osmanović,\* Ian J. Ford, and Bart W. Hoogenboom

London Centre for Nanotechnology and Department of Physics and Astronomy, University College London, London, United Kingdom

**ABSTRACT** Nuclear transport receptors (NTRs) mediate nucleocytoplasmic transport via their affinity for unstructured proteins (polymers) in the nuclear pore complex (NPC). Here, we have modeled the effect of NTRs on polymeric structure in the nanopore confinement of the NPC central conduit. The model explicitly takes into account inter- and intramolecular interactions, as well as the finite size of the NTRs (~20% of the NPC channel diameter). It reproduces various proposed scenarios for the channel structure, ranging from a central polymer condensate (selective phase) to brushlike polymer arrangements localized at the channel wall (virtual gate, reduction of dimensionality), with the transport receptors lining the polymer surface. In addition, it predicts a new structure in which NTRs become an integral part of the transport barrier by forming a cross-linked network with the unstructured proteins stretching across the pore. The model provides specific and distinctive predictions for the equilibrium spatial distributions of NTRs for these different scenarios that can be experimentally verified by, e.g., superresolution fluorescence microscopy. Moreover, it suggests mechanisms by which globular macromolecules (colloidal particles) can cause polymer-coated nanopores to switch between open and closed configurations, a possible explanation of the biological function of the NPC, and suggests potential technological applications for filtration and single-molecule sensing.

## INTRODUCTION

The nuclear pore complex (NPC) is the sole gate for macromolecular transport between the nucleus and the cytoplasm of eukaryotic cells (1–7). It consists of a large scaffold spanning the nuclear envelope, with an outer diameter of 90–120 nm and a central channel or conduit of diameter 30–50 nm for transport. Although the scaffold structure consists of structural nucleoporins (nups) and is reasonably well defined, the proteins in the central channel are largely unstructured and disordered, which compromises the results yielded by conventional methods of structure determination that rely on crystal formation and symmetry-facilitated averaging. These unstructured proteins are anchored to the NPC scaffold structure and contain multiple repeats of Phe-Gly dipeptides (often referred to as FG nups). The NPC contains FG nups with various properties (8,9), where cohesive nups have been shown to be essential for NPC function (10). They form a barrier that allows passive diffusion of solutes <6 nm in diameter but prevents passage of inert molecules >9 nm in diameter unless they are chaperoned by nuclear transport receptors (NTRs) (8). All macromolecules (cargos) that are transported through the pore contain a nuclear localization signal or a nuclear export signal that binds to an NTR and the NTR-bound cargo can then diffuse through the pore.

Transport of cargos through the NPC critically depends on the intermolecular interactions between NTRs and nups. NTRs bind to the FG domains of nups via hydrophobic interactions, which must be finely calibrated to allow translocation and final detachment (11,12). Key questions on NPC function focus on the nature of the transport barrier, i.e., whether the FG nups form a predominantly entropic or energetic barrier to unspecific transport, and on the role of structural heterogeneity in the NPC.

The NPC can thus be regarded as a complex version of a polymer-coated nanopore, a structure of significant technological (13) and physical interest. It has inspired biomimetic devices, in which solid-state nanopores are coated with selected proteins from the NPC central channel (14,15). In general, artificial solid-state nanopores enable the detection of single molecules through changes in ionic currents through (16,17) or across (18) them. Nanopores can also be used as molecular filtration devices, with applications from separating biomolecules to water purification (19). In addition, nanoporous devices have been used as novel drug-delivery devices (20). Transport selectivity is one of the key challenges in the application of nanopores. Although size exclusion is reasonably straightforward, chemical selectivity is harder to achieve. One strategy for achieving better control of single-molecular transport is by functionalization of the pores with one-end-grafted polymers of the NPC (15,21,22).

The physical interest lies in the various types of behavior that arise because of polymer/polymer interactions in the confinement of a cylindrical nanopore. The collective behavior of such polymers yields a wide and rich pattern of possible morphologies, which is critically dependent on the interaction parameters, as has been

Submitted July 2, 2013, and accepted for publication November 4, 2013.

\*Correspondence: [d.osmanovic@ucl.ac.uk](mailto:d.osmanovic@ucl.ac.uk)

This is an Open Access article distributed under the terms of the Creative Commons-Attribution Noncommercial License (<http://creativecommons.org/licenses/by-nc/2.0/>), which permits unrestricted noncommercial use, distribution, and reproduction in any medium, provided the original work is properly cited.

Editor: R. Astumian.

© 2013 The Authors  
0006-3495/13/12/2781/9 \$2.00



demonstrated by numerical simulations (23–27). For the NPC, these and other models (28) have a major shortcoming in not incorporating the presence of NTRs in the pore. Experimental data suggest the simultaneous presence of tens if not hundreds of transport receptors per NPC under physiological conditions (29), which would correspond to a significant fraction of the available volume in the NPC central channel. NTRs have also been suggested as integral components of the NPC selectivity barrier (14,30,31). In this work, we therefore set out to explore the effects of NTRs on the polymeric structure in the NPC channel. This work can be compared directly to superresolution fluorescence microscopy measurements of positions of proteins within the NPC, along the lines of Lowe et al. (32)

## METHODS

The studied system consists of 40 polymers of 100 nm stretched length that are one-end grafted to a ring inside an open-ended, hollow, and impermeable cylinder of 50 nm diameter, in the presence of a fluid of large, spherical colloidal particles to represent NTRs (see Fig. 1). The diameter of the colloidal particles is set to 8 nm, corresponding to the unhydrated diameter of NTRs (33). The polymers are treated as freely jointed chains of identical connected and interacting beads, with a Kuhn (segment) length identical to the bead diameter of 1 nm. They represent a simplified version of the NPC (27), neglecting much of its molecular-scale heterogeneity, such that it is computationally feasible to study the system over a wide range of parameters. This is a significant advantage, since the outcome of numerical models for polymer-coated nanopores critically depends on parameter settings (28). We first study the effects of the colloidal particles on polymers in this minimal model, which are consistent with our previously published polymer distributions (27). Next, we verify how these effects translate to a more complex polymer distribution that better represents the NPC. As will be demonstrated below, the

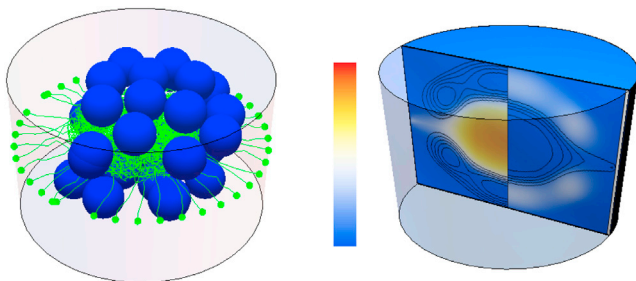


FIGURE 1 (Left) Snapshot of a Monte Carlo simulation of 40 polymers consisting of 100 adjacent beads (green), each tethered on a ring around the inner surface of a cylinder to represent FG nups in the NPC. Free colloidal particles (blue spheres) are included to represent NTRs. (Right) Cross section of the cylinder with the molecular packing fraction, resulting from a density functional theory calculation of the same system, assuming rotational symmetry around the cylindrical axis. On either side of the axis of symmetry, the color illustrates the proportion of the space that is filled by polymers (left, with contour lines illustrating the density of the globular macromolecules) and colloidal particles (right, with contour lines illustrating the density of polymers), respectively, for a particular choice of the interaction parameters. To see this figure in color, go online.

model reproduces the various qualitatively different scenarios for the structure of the NPC transport barrier by only minor variations in parameters for intermolecular interactions. We therefore argue that despite its minimalistic nature, this model can capture the key physical behaviors that can occur in the NPC.

Classical density functional theory is used to calculate polymer and colloidal particle densities, and the densities are assumed to be rotationally symmetric around the central axis of the pore. This model is based on a free-energy functional similar to that used in our previous work (27) but extended by the application of fundamental measure theory (34) to accurately describe the density of finite-sized hard spheres. The use of such a nonlocal functional is necessary because of the large size asymmetry between the polymer beads and the colloidal particles, and because the size of the colloidal particles cannot be neglected compared to the pore diameter.

We construct a semigrand potential of the system, which is a functional of the density of the polymer beads and the colloid density:

$$\beta\Omega = \beta F_p[W(\mathbf{r})] + \beta\Omega_c[\rho_c(\mathbf{r})] + \beta F_{pc}^{int}[W(\mathbf{r}), \rho_c(\mathbf{r})], \quad (1)$$

with  $\beta = 1/k_B T$ .  $k_B$  is the Boltzmann constant and  $T$  is the temperature, as usual. This is a functional of the colloid density,  $\rho_c$ , and the polymer mean field,  $W$ . Given that the polymer density and the polymer mean field are different representations of the polymers, the functional is implicitly a functional of the polymer density as well.

The term  $F_p$  describes the free energy of  $M$  polymers made up of point-like beads in an external potential,  $V_p$ :

$$\beta F_p[W(\mathbf{r})] = -M \ln Z[W(\mathbf{r})] - \int W(\mathbf{r})\rho_p(\mathbf{r}) \, d\mathbf{r} + \int V_p(\mathbf{r})\rho_p(\mathbf{r}) \, d\mathbf{r}. \quad (2)$$

$V_p$  defines an external potential acting on the polymers.  $W(\mathbf{r})$  is the polymer mean field that is to be adjusted to best represent the interparticle interactions between the polymer beads. This mean field is defined on a cylindrically discretized grid in  $r$  and  $z$ , with 40 and 61 grid points, respectively. The cylinder is of radius 25 nm and height 60 nm.  $\rho_p$  is the density of beads making up the polymer.  $Z[W(\mathbf{r})]$  is the canonical partition function of a single polymer in the total potential comprising  $W(\mathbf{r})$  and  $V_p$ .

The term  $\beta\Omega_c[\rho_c(\mathbf{r})]$  describes an ideal fluid of colloidal point particles interacting with an external potential:

$$\beta\Omega_c[\rho_c(\mathbf{r})] = \int \rho_c(\mathbf{r})(\ln(\lambda^3 \rho_c(\mathbf{r})) - 1) \, d\mathbf{r} + \int V_c(\mathbf{r})\rho_c(\mathbf{r}) \, d\mathbf{r} - \mu \int \rho_c(\mathbf{r}) \, d\mathbf{r}, \quad (3)$$

where  $\rho_c$  is the density of colloidal particles, defined on a  $426 \times 1024$  mesh in  $r$  and  $z$ ;  $\lambda$  is the thermal de Broglie wavelength;  $\mu$  is the chemical potential of the colloidal particles; and  $V_c$  is the external potential applied onto the colloids. Within the context of this work, these external potentials are used to define the differing geometrical constraints placed on the particles. As the colloidal particles are larger, their centers cannot be as close to the wall as the centers of the polymer beads, we represent this by imposing a large repulsive external potential  $V_c(r, z)$  when  $r > R_{\text{cylinder}} - R_{\text{colloid}}$ .

Finally, the term  $\beta F_{pc}^{int}[W(\mathbf{r}), \rho_c(\mathbf{r})]$  accounts for all the attractive and repulsive interactions in the system

$$\begin{aligned}
F_{pc}^{int}[W(\mathbf{r}), \rho_c(\mathbf{r})] = & \iint \rho_p(\mathbf{r})\rho_c(\mathbf{r}')\phi_{pc}^l(\mathbf{r}-\mathbf{r}')d\mathbf{r}d\mathbf{r}' \\
& + \int d\mathbf{r} \{ \Phi^{HS}[\{n_\alpha\}](\mathbf{r}) \\
& + \Phi^{ch}[\{n_\alpha\}](\mathbf{r}) \} \\
& + \frac{1}{2} \iint \rho_c(\mathbf{r})\rho_c(\mathbf{r}')\phi_{cc}^l(\mathbf{r}-\mathbf{r}')d\mathbf{r}d\mathbf{r}' \\
& + \frac{1}{2} \iint \rho_p(\mathbf{r})\rho_p(\mathbf{r}')\phi_{pp}^l(\mathbf{r}-\mathbf{r}')d\mathbf{r}d\mathbf{r}'.
\end{aligned} \tag{4}$$

The term  $\Phi^{HS}$  is a dimensionless excess free-energy density due to the hard-sphere repulsion. The next term  $\Phi^{ch}$  gives an excess free-energy density due to the fact that the hard spheres comprising the polymers are connected as a set of chains. These terms depend on a set of weighted densities,  $\{n_\alpha\}$  (34). The remaining terms account for attractive interactions in the system via a generic potential,  $\phi_{ij}^l(\mathbf{r})$ , for the physical interaction between a particle of species  $i$  and another particle of species  $j$ . This potential is given by

$$\phi_{ij}^l(\mathbf{r}) = \begin{cases} 0 & |\mathbf{r}| < R_i + R_j \\ -\epsilon_{ij}\exp(-(|\mathbf{r}| - (R_i + R_j))/\sigma_{ij}) & |\mathbf{r}| \geq R_i + R_j, \end{cases} \tag{5}$$

where  $\epsilon_{ij}$  is the strength of the interaction in units of  $k_B T$  ( $\epsilon_{ij} > 0$ ),  $\sigma_{ij}$  is its range in units of nm, and  $R_i$  and  $R_j$  are the hard sphere radii of species  $i$  and  $j$ , respectively. The superscript  $l$  is to show that we only consider the long-range interactions of the pair potential, and the hard-sphere repulsion is represented through the hard-sphere term.

Note that the functional of the polymer density (Eq. 2) is a free energy, as there is a fixed number of polymers in the system. However, the functional of the colloid density (Eq. 3) is a grand potential, as the colloid is allowed to undergo particle exchange with an external reservoir. We make this explicit by using  $F$  to describe the functional of the polymer density and  $\Omega$  to describe the functional of the colloid density. Thus, the full thermodynamic potential describing the system is semigrand. This functional can be minimized numerically to provide the best estimate of the equilibrium polymer and colloid densities within the system. Further details about the semigrand potential and its derivation can be found in the [Supporting Material](#).

This functional includes hard-sphere (excluded-volume) interactions between the polymer beads and the colloidal particles, as well as attractive polymer/polymer, polymer/colloid, and colloid/colloid interactions of strengths  $\epsilon_{pp}$ ,  $\epsilon_{pc}$ , and  $\epsilon_{cc}$ , respectively. The range  $\sigma$  for the attractive interactions is set to be 1 nm and  $\epsilon_{cc} = 0$ , i.e., there is no condensation of the colloidal particles in the absence of the polymers. For the colloidal particles, an excess chemical potential is referenced with respect to the chemical potential ( $\mu_{ex} = 0$ ) that yields a colloidal particle bulk density of  $6 \times 10^{-6} \text{nm}^{-3}$ , equivalent to 10  $\mu\text{M}$ , the approximate concentration of NTRs in the cytoplasm (35). An excess chemical potential  $\mu_{ex} = \pm 2$  corresponds to an  $\sim 10$ -fold increase/decrease of the bulk concentration.

## RESULTS

We represent the polymer/colloid densities on a vertical cross section through the pore as illustrated in Fig. 1. We subdivide this cross section into two sides through the  $r = 0$  axis of symmetry. On the lefthand side, we plot the packing fraction of the polymers on a false color scale, overlaid with a contour map of the colloidal particle packing

fraction. On the righthand side, we plot the packing fraction of the colloidal particles and overlay a contour map of the polymer packing fraction. The false color scale in all plots is unitless and is fixed to range from 0 to 1. All the plots are reproduced in the [Supporting Material](#) on color scales that are optimized for each density plot to emphasize the approximate positions of the components.

As in our previous calculations (27), we find that tethered polymers have multiple phases when the colloidal particle density is small (Figs. 2 and 3, upper rows). Broadly, one can categorize the resulting polymer density as either a wall phase, where the majority of polymers are near their tethering point at the wall, or a central phase, where the polymers stretch away from their anchoring point to meet in the center of the cylinder. Depending on the parameters, only one of these two phases is stable, whereas the other can exist as a metastable solution of the system. The central phase becomes more stable on increasing the interpolymer interaction. If the attraction is not strong enough, the wall phase will be favored. There is a crossover in the free energies of the central phase and the wall phase. This crossover can be understood from the balance between the energetic cost of keeping interacting polymers apart on one hand, and the entropic cost of stretching the polymers toward the center on the other. Provided that the interaction strength is strong enough, the entropic cost of stretching the

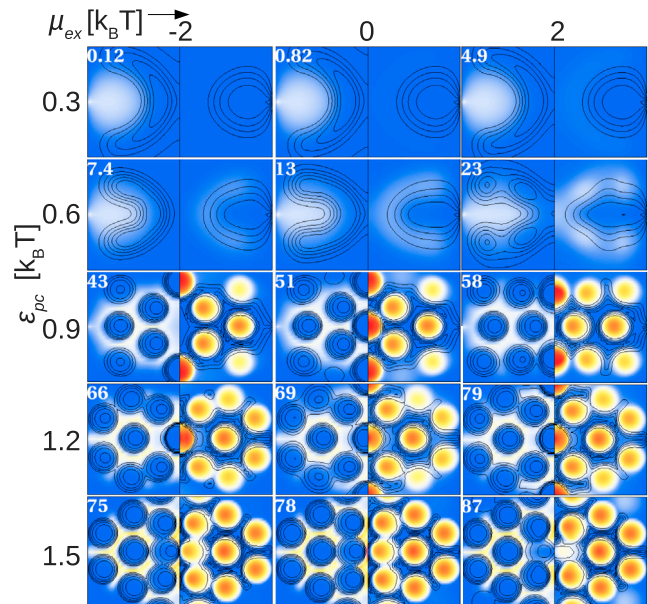


FIGURE 2 Equilibrium polymer and colloid packing fractions represented on vertical cross sections of the pore for a polymer/polymer interaction ( $\epsilon_{pp} = 0.05 k_B T$ ) that yields a wall phase in the absence of colloids. The colloid bulk concentration is made to increase in order-of-magnitude steps via  $\pm 2$  changes in  $\mu_{ex}$  from left to right, and the polymer/colloid interaction,  $\epsilon_{pc}$ , increases from top to bottom. The data representation is as explained in Fig. 1, and the number in each cross-sectional image indicates the average number of colloids in the pore. To see this figure in color, go online.

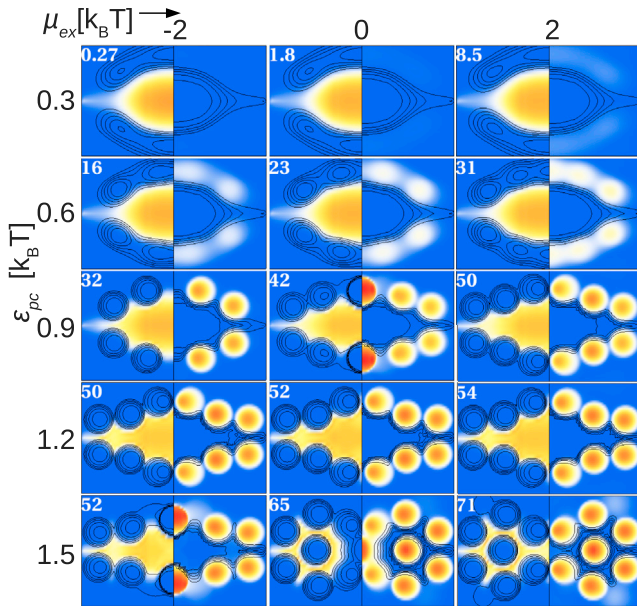


FIGURE 3 Equilibrium polymer and colloid packing fractions represented on vertical cross sections of the pore, for a polymer/polymer interaction ( $\epsilon_{pp} = 0.10 k_B T$ ) that yields a central polymer condensate in the absence of colloids. The colloid bulk concentration is made to increase in order-of-magnitude steps via  $\pm 2$  changes in  $\mu_{ex}$  from left to right, and the polymer/colloid interaction,  $\epsilon_{pc}$ , increases from top to bottom. The data representation is as explained in Fig. 1, and the number in each cross-sectional image indicates the average number of colloids in the pore. To see this figure in color, go online.

polymers can be compensated by the resulting gain in binding energy. For this work, we have chosen a range of interpolymer interaction strengths that are physiologically relevant, which coincides with the range where the polymers are near to this wall/central-phase boundary, where we also anticipate the most interesting physical and eventually technological behavior will occur.

Figs. 2 and 3 give an overview of the effect of the colloidal particles on the polymer distribution for polymer/polymer interactions ( $\epsilon_{pp}$ ) that, in the absence of colloidal particles, yield wall and central phases, respectively. Several general features of the polymer/colloid distributions can be observed. As expected, the pores become more filled on increasing the polymer/colloid attraction or increasing the bulk concentration of the colloidal particles. This is apparent from the increasing number of colloidal particles in the pore, as well as from the color maps (where blue corresponds to zero packing fraction).

In addition, stronger polymer/colloid attraction causes greater localization of the colloidal particles at certain favored positions, as can be seen in  $\epsilon_{pc} \gtrsim 0.6 k_B T$  in Figs. 2 and 3. When the attraction between the colloidal particles and the polymers is strong enough relative to the interpolymer attraction, it is thermodynamically favorable to form a quasilattice structure. Different kinds of packing are observed, where the colloidal particles can be arranged

into pentagonal or hexagonal structures. The spaces between the colloidal particles are filled with polymers, which act as a glue that holds the colloidal particles together. As the colloidal particles have no attraction to one another, they are held in the lattice only by their attraction to the polymers. This is analogous to metallic bonding, where positive metal ions are held in a regular structure through their attraction to a sea of (negatively charged) electrons. It should be stressed that these structures are the equilibrium, minimum-free-energy solutions. In reality, dynamic phenomena, such as polymer entanglement, might frustrate the formation of these phases, possibly leading to nonequilibrium, amorphous glassy states.

For  $\epsilon_{pc} > 1.5 k_B T$ , density of the colloidal particles increasingly resembles a collection of delta functions centered at a few very specific positions. In practice, this leads to increasing numerical inaccuracies and corresponding difficulties in converging to the minimum-free-energy solutions. Hence, we have here restricted our observations and conclusions to  $\epsilon_{pc} \leq 1.5 k_B T$  here, noting that for stronger polymer/colloid interactions, the general trends appear to continue: accumulation of colloidal particles at sharply defined positions in a lattice.

A consistent feature of all the calculations is the low polymer/colloid miscibility. Regions where there is a large packing fraction of polymers are unlikely to have a significant packing fraction of colloidal particles, and vice versa. It is entropically unfavorable for polymers and large molecules to mix due to the large reduction in possible conformations of a tethered polymer when there is a large particle near it. Colloids and polymers have poor miscibility in general (36), until the polymer/colloid interactions are strong enough to overcome the entropic costs of interspersing polymers with finite-size colloidal particles. Not surprisingly, this transition occurs more readily ( $\epsilon_{pc} \gtrsim 0.9 k_B T$ , Fig. 2) for weaker polymer/polymer interactions than for the stronger polymer/polymer interactions that—in the absence of colloidal particles—yield a central polymer condensate for low polymer/colloid interactions (in which case the transition occurs at  $\epsilon_{pc} \gtrsim 1.5 k_B T$ ; Fig. 3).

We observe a few other effects that are more specifically dependent on the interpolymer attraction strength. In Fig. 2, the strength of this attraction is such that in the absence of the colloidal particles, the polymers are in a wall phase, leaving an aperture along the central axis of the channel. The addition of the colloidal particles initially ( $\epsilon_{pc} = 0.6 k_B T$ ) leads to a moderate blocking (clogging) of the central aperture by the colloidal particles, until, for  $\epsilon_{pc} \gtrsim 0.9 k_B T$ , the earlier-mentioned polymer/colloid lattice is formed, completely blocking the pore.

When the interpolymer attractions are strong enough to form a central phase, as in Fig. 3, the colloidal particles have more difficulty in penetrating into the polymer network. Nevertheless, the colloidal particles still become increasingly localized with increasing polymer/colloid

attraction, but only on the surface of the polymer condensate. Once the polymer/colloid attraction is strong enough, the familiar lattice formation is observed.

In Fig. 4, we illustrate that the system can, for identical parameter settings, converge to different states. Some of these states will be metastable. The relative stability of these phases can be tuned via the polymer/colloid interaction. In the case for  $\epsilon_{pp} = 0.07$ , we see a crossover in the free energies of the centrally condensed state and the wall condensed state, where the centrally condensed state becomes more stable. In the complete absence of colloidal particles (the bulk density of the colloidal particles being zero), the wall phase is favored. The addition of colloidal particles of a certain attraction to the polymers will make the central state favored. They cause the pore to switch from an open to a closed state.

In Fig. 5, we show the grand potential of the system as the polymers and colloidal particles begin to mix to form polymer/colloid networks. There are increasingly rapid changes in the grand potential as the polymer/colloid interaction crosses the threshold necessary for the polymers and the colloidal particles to mix, at  $\epsilon_{pc} \approx 0.7$ , with a corresponding large increase in the number of colloidal particles found in the system.

The results thus far are summarized in Fig. 6, which shows the approximate regions of stable phases against the interpolymer and polymer/colloid interactions. We subdivide the observed phases into three rough categories: the two familiar central/wall phases described previously (27),

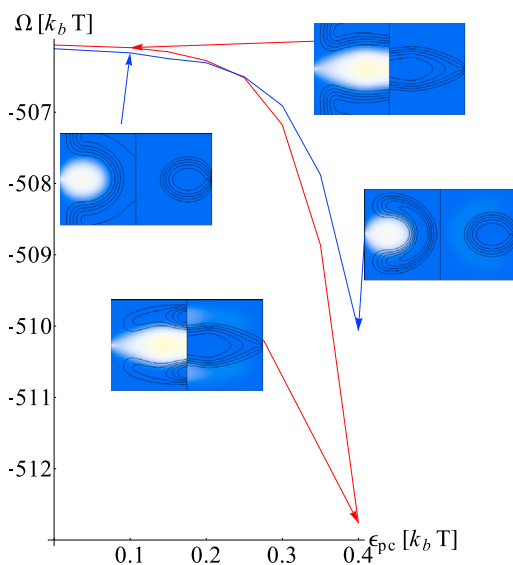


FIGURE 4 Polymers in the nanopore switching between (meta)stable open and closed configurations. The plot indicates the grand potential of wall and central polymer phases as a function of the polymer/colloid interaction,  $\epsilon_{pc}$ , for a given  $\epsilon_{pp} = 0.07 k_B T$  and  $\mu_{ex} = 0$ . The presence of low amounts of colloidal particles in the pore stabilizes the central phase for  $\epsilon_{pc} \gtrsim 0.25 k_B T$ , at the expense of the wall phase. Polymer and colloid packing fractions are represented as in Figs. 1–3. To see this figure in color, go online.

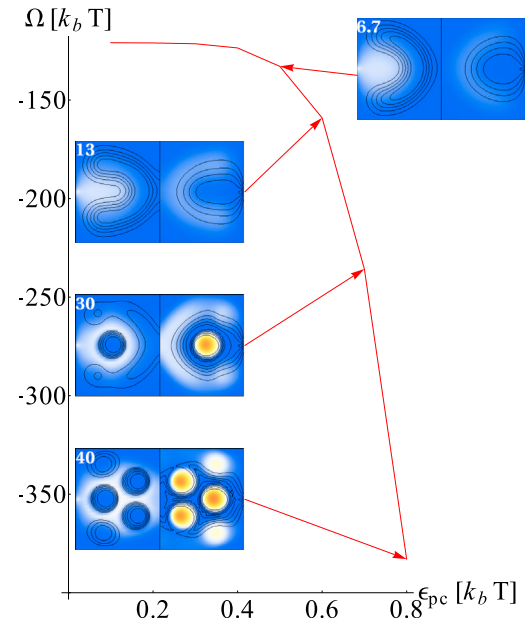


FIGURE 5 Transition of a wall state into a polymer/colloidal-particle network, plotted are the grand potentials against polymer/colloid attraction for  $\epsilon_{pp} = 0.05$  and  $\mu_{ex} = 0$ . Large attractions between the polymers and the colloidal particles cause the formation of polymer-colloid networks. To see this figure in color, go online.

and a third phase where the interactions between the polymers and the colloidal particles is strong enough to form a lattice structure, as can be seen at the lower parts of Figs. 2 and 3. Increasing the polymer/colloid interaction has the effect of stabilizing the central phase at the expense of the wall phase. In general, as one increases the polymer/colloid attraction, such that the ratio of the interpolymer interaction to the polymer/colloid interactions becomes

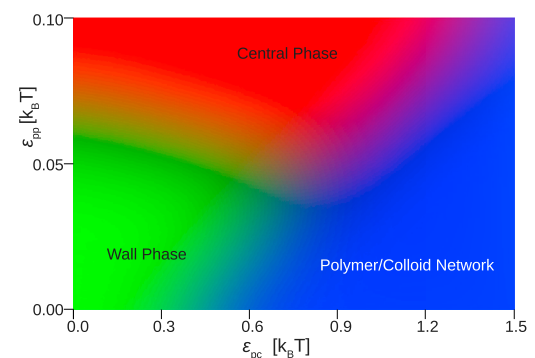


FIGURE 6 Approximate phase map of the combined polymer/colloid system at different  $\epsilon_{pp}$  and  $\epsilon_{pc}$ , showing the most stable phase for these different parameters at  $\mu_{ex} = 0$ . The wall phase is reminiscent of brushlike polymer arrangements localized at the channel wall (e.g., virtual-gate and reduction-of-dimensionality models for the NPC); the central phase corresponds to a cohesive polymer condensate blocking the pore (selective-phase model for the NPC); and the polymer/colloid network emerges from our calculations for large numbers of NTRs in the NPC, as suggested by experiment. To see this figure in color, go online.

small, lattice states will form. These phases are not homogeneous, as the colloidal particles can be arranged in different types of lattices.

These have all been obtained for attractive polymer/colloid interactions. In the absence of such interactions, very few colloidal particles enter the pore (see [Supporting Material](#)).

The results thus far have been obtained for a single polymer layer in a cylindrical nanopore. Having explored the different types of behavior for this simple model system, we next investigate whether it is reproduced in a system that more closely resembles the nups in the NPC central channel. As before, we set a channel diameter to 50 nm but tether the polymers uniformly over a range of 30 nm (centered around  $z = 0$ ) to more closely resemble the vertebrate NPC structure (7). The 216 nups in the channel are approximated as chains of beads 0.76 nm diameter (consistent with twice the 0.38 nm average length/amino acid in nups), and a total stretched length of 161 nm, the average of the contour length of the FG domains in the human NPC (37).

Trends similar to those seen previously are apparent. The more realistic treatment of the geometry will clearly make a quantitative difference to the location of phase boundaries seen in [Fig. 6](#), but the qualitative structure of the boundaries will remain. The increases in the number of polymers and polymer length have made the central phase more stable, despite the decrease in bond length and particle diameter and the smearing out of the polymer tethering points, which taken alone would make the wall phase more favorable. As such, the central/wall dichotomy of structures seen in the previous calculations still exists, but is less readily apparent, as even at weak interactions  $\epsilon_{pp} = 0.05$  the polymers will extend into the central channel. However, increasing the number of polymers appears to make intermixing between the colloidal particles and polymers less likely; the formation of lattice states appears to be frustrated when the polymers are attractive to one another, and the colloidal particles appear to be more localized on the polymer surface. That is, when  $\epsilon_{pf} = 1.0$ , we find a lattice state in the single polymer layer, but a centrally condensed polymer phase in [Fig. 7](#). At low polymer/polymer affinity, lattice states are observed in [Fig. 7](#), as the colloidal particles can more readily penetrate the polymers. The change in the tethering conditions also results in a larger number of colloidal particles in the pore.

## DISCUSSION

We have established that a system of tethered interacting polymers in the presence of attractive spherical macromolecules can adopt a rich range of configurations inside a cylindrical pore. Much of our motivation for this study was to determine whether biological function can be related to such physical behavior. The selectivity of nucleocytoplasmic

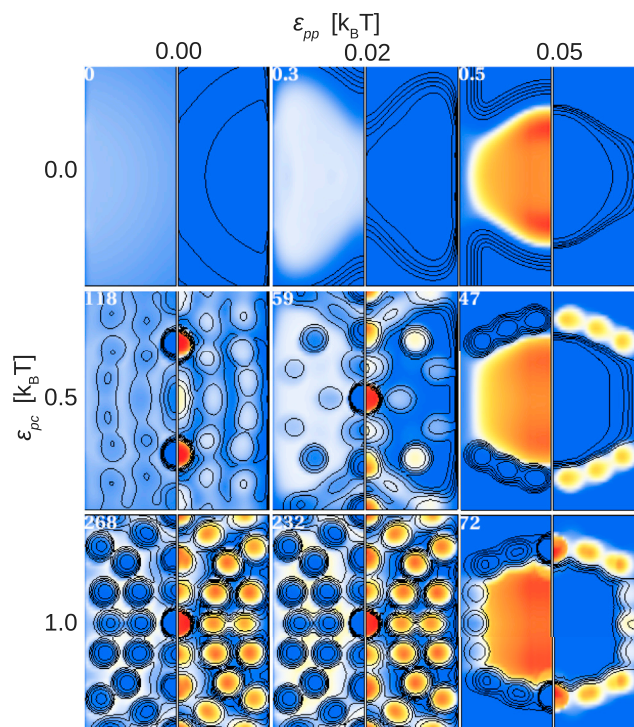


FIGURE 7 Equilibrium polymer and colloid packing fractions for a polymer tethering distribution that more closely matches the NPC structure. The results are represented by vertical cross sections of the pore for different strengths of polymer/polymer and polymer/colloid interactions. For clarity, the results are displayed over twice the vertical ( $z$ ) range relative to [Figs. 1–6](#). To see this figure in color, go online.

transport of biomolecules through the NPC is a particular feature that requires explanation, and it has been alluded to here and in our previous article (27) that a pore where the polymers reside near the wall is more open for transport (less selective) than a pore where polymers accumulate near the axis. We have now shown, using our simplified model, that free quasispherical macromolecules affect this open or shut behavior in a complex fashion, and that they can also penetrate a centrally condensed polymer plug to form a composite mixture with potentially distinct physical properties.

In general, we find that the presence of colloidal particles can cause a complete shift in polymer density profiles in a nanopore; that significant rearrangements of the polymer/colloid configuration can be induced by marginal changes ( $\leq 0.1 k_B T$ ) in interaction strength; and that several metastable phases can be observed. As illustrated in [Figs. 2–5](#), the structure of polymers and colloidal particles in nanopores can be very rich. This richness can be attributed to the combined effects of confinement and complex many-particle interactions.

The equilibrium structures here presented enable us to qualitatively discuss various possible mechanisms of selective and tunable macromolecular/colloidal transport through polymer-coated nanopores. In one scenario, colloidal particles with a weak polymer affinity will move relatively freely

into an open central aperture (Fig. 2, upper rows) while blocking the aperture for noninteracting particles. Such colloidal particles may also be used to tune the size-exclusion limit for noninteracting particles by deliberately narrowing the central aperture in the pore. In another scenario (Fig. 4), colloidal particles with weak polymer affinity can cause the polymers to stretch across the pore, thus blocking all macromolecular transport that in the absence of these particles might be allowed. For larger polymer/colloid affinity, colloidal particles can be used to break through a polymer condensate or central phase (Fig. 3, lower rows), thus facilitating transport that is otherwise inhibited along the central axis of the pore.

It is important to note that as a consequence of the assumption that the density profiles of both polymers and colloidal particles are azimuthally symmetric, the phases here would be slightly modified if the calculations were performed in three dimensions. In our previous article (27), the effect of the relaxation of the azimuthal symmetry condition was explored. The system can break the symmetry when there are attractive interactions between the polymers (38), forming distinct clumps at the wall. However, the important dichotomy of central/wall phases remains. It should be noted, of course, that the network phases observed in this study would become full lattices in three dimensions.

In the biological context of the NPC, we can identify several of the previously proposed paradigms for the transport barrier. For low nup/nup (polymer/polymer) interactions and little affinity between nups and NTRs (Fig. 6, Wall Phase), the nups will be in the wall phase and the transport barrier will be predominantly entropic in nature (39). Such a moderate affinity between nups and NTRs will not significantly change the nups structure (Fig. 2, upper rows). The NTRs will not mix with the nups but will coat their surface, reducing or blocking the central aperture of the pore and discouraging unspecific transport. In such a model, the NTRs would form a key part of the selectivity barrier blocking the transport of inert molecules. However, such a model might contravene experimental evidence, as in digitonin-permeabilized cells most NTRs are washed out of the cell, yet the barrier to inert molecules is still observed to be functioning (40). This parameter range is also reminiscent of the reduction-of-dimensionality model (41), which postulates that cargoes, when bound to NTRs, slide over the surface of the nups in a roughly one-dimensional random walk along the NPC central axis.

For stronger nups/nups interactions and low to moderate affinity between nups and NTRs (Fig. 6, Central Phase), the nups will form a condensate that stretches across the NPC channel. The barrier to transport will thus be predominantly energetic, as proposed in the selective-phase model (42). Such a nups structure will be more resistant to penetration by NTRs (Fig. 3, upper rows), which will mainly be found on the surface of the nups condensate, and effectively

follow a bimodal distribution as a function of vertical position in the pore, as indeed is reported by superresolution fluorescence microscopy for 18-nm-diameter quantum dots (32) and for NTRs (31,43). Selective transport may be facilitated by the presence of a metastable wall phase for the nups, especially if the free energy difference between the wall and central phases is small. At present, the role of NTRs in such a rearrangement is difficult to gauge from these calculations, not least because they seem to promote a transition from wall to central phase, the opposite of what would be required for transport (Fig. 4).

Experiments suggest that the NPC can accommodate up to 100 NTRs (29), which is a three-orders-of-magnitude enhancement of the local receptor concentration in the NPC compared to the concentration within the cell. Such large numbers of NTRs only accumulate in the pore for relatively high affinity between nups and NTRs, and they appear to be more compatible with the central phase (Fig. 3) or the polymer/colloid networks formed when the NTRs penetrate the nups (Figs. 2 and 3, lower rows). The latter case (Fig. 6, Polymer/Colloid Network) would correspond to a gel-like state, as proposed in the selective-phase model, but with the NTRs playing a significant role in its cohesiveness. The NPC central channel would thus act as a potential well rather than a potential barrier for NTRs, but the free-energy costs of nup rearrangement for cargo transport may be significant. It is also worth noting that in this parameter range, the number of NTRs in the NPC is only moderately dependent on their concentration in the surrounding liquid:  $\pm 10 \sim 20\%$  for an  $\sim 10$ -fold increase/decrease in bulk concentration ( $\mu_{ex} = \pm 2k_B T$ ).

Taken together, these observations indicate that different proposed models for transport correspond to distinctly different behavior of NTRs in the NPC. This is particularly interesting because recently developed superresolution fluorescence microscopy techniques (31,32,43–47) now increasingly yield experimental access to single-molecule probability distributions during transport events, and in some cases to the NTR distributions (31,43), as noted above.

Finally, our results call for caution in defining parameters for modeling any polymer-coated nanopores, since small changes in parameters can lead to significant changes in polymer behavior, in particular in the presence of macromolecules or other colloidal particles with affinity for the polymers. In addition, the presence of well-defined metastable states implies that modeling results need to be carefully examined to establish the correct equilibrium configurations of the system. Obviously, when attempting to extrapolate our model to the NPC, we have ignored various complicating biological factors, such as the chemical heterogeneity of the polymers or the exact hourglass shape of the NPC channel. A fully realistic treatment of the NPC would have to incorporate all of these aspects but would also need an accurate specification of the

parameters involved, which makes for an ungainly combination of an ever-expanding phase space for the model and the need to make exact predictions of biological behavior. Although the quantitative nature of our results would change were we to account for full biological complexity, we expect the characteristics of the phases observed to remain similar. This is illustrated by the comparison between our minimal single-polymer-layer model and a polymer-tethering distribution that more closely resembles the NPC: the qualitative picture—wall/central dichotomy and lattice states—remains the same despite significant changes in factors such as tethering positions and polymer lengths.

## CONCLUSION

To explore the effect of NTRs on the structure in the NPC central channel, we have modeled, over a physiologically reasonable parameter range, the equilibrium density of an asymmetric mixture of finite-sized colloidal particles and tethered polymers within a nanopore. The resulting density profiles share some common features with previously found polymer morphologies in nanopores (23,27), such as polymer density accumulation at the pore wall (wall phase) and—overcoming the entropic costs of stretching the polymers—polymer condensation at the pore center (central phase), as well as the emergence of various metastable states from our calculations.

It is also demonstrated that the interaction with colloidal particles can cause significant rearrangement of the polymers by switching them between the open-pore wall phase and the closed-pore central phase, as well as via the emergence of a new phase in which the colloidal particles penetrate the polymers, forming a tightly bound polymer/colloid network with highly ordered colloid lattices as the state of lowest free energy. These structures are physically interesting for the analogy one can draw with metals, with the polymers holding the colloidal particles together in a way reminiscent of free electrons binding metal ions. However, such networks are only formed for higher polymer/colloid affinities, as the miscibility of the polymers and colloidal particles is generally found to be low.

Based on the equilibrium packing fractions in the nanopore, one can conclude that the presence of colloidal particles will significantly affect its transport properties. Unspecific transport can be reduced by a clogging of the wall phase, thus tightening the predominantly entropic selectivity barrier, but also, less trivially, by the switching to central or polymer/colloid network phases, where the selectivity barrier is predominantly energetic. Transport through such energetic barriers may be facilitated by the colloidal penetration of the polymers and/or by the existence of various metastable phases, particularly if the free-energy differences between them are small.

These results specifically demonstrate that the distribution of NTRs in the NPC is a key distinctive feature of the various models that have been proposed to explain the biological function of the NPC, namely, its selectivity of biomolecular transport. Given the large number of transport receptors that have been reported experimentally (29), the polymer/colloid (nups/transport receptor) network phase, or a nup barrier thickly coated with NTRs, emerges as a likely state in the NPC central channel. Although the likelihood of one of these states cannot be obtained a priori from this work, we anticipate that it will guide the interpretation of future high-resolution experiments on the distribution of NTRs in the NPC. Furthermore, it can be expanded to estimate free-energy barriers to transport and to include the here-ignored structural heterogeneity of FG nups in the NPC (48).

## SUPPORTING MATERIAL

Five figures and a description of the model and theory are available at [http://www.biophysj.org/biophysj/supplemental/S0006-3495\(13\)01242-3](http://www.biophysj.org/biophysj/supplemental/S0006-3495(13)01242-3).

We gratefully acknowledge A. Lowe, A. Fassati, J. Edel, P. Sushko, and B. Evans for discussions. The authors acknowledge the use of the UCL Legion High Performance Computing Facility (Legion@UCL), and associated support services, in the completion of this work.

This work was funded by the Sackler Foundation.

## REFERENCES

1. Grünwald, D., R. H. Singer, and M. Rout. 2011. Nuclear export dynamics of RNA-protein complexes. *Nature*. 475:333–341.
2. Hoelz, A., E. W. Debler, and G. Blobel. 2011. The structure of the nuclear pore complex. *Annu. Rev. Biochem.* 80:613–643.
3. Kahms, M., J. Hüve, ..., R. Peters. 2011. Lighting up the nuclear pore complex. *Eur. J. Cell Biol.* 90:751–758.
4. Onischenko, E., and K. Weis. 2011. Nuclear pore complex, a coat specifically tailored for the nuclear envelope. *Curr. Opin. Cell. Biol.* 23:293–301.
5. Aitchison, J. D., and M. P. Rout. 2012. The yeast nuclear pore complex and transport through it. *Genetics*. 190:855–883.
6. Bilokapic, S., and T. U. Schwartz. 2012. 3D ultrastructure of the nuclear pore complex. *Curr. Opin. Cell Biol.* 24:86–91.
7. Grossman, E., O. Medalia, and M. Zwerger. 2012. Functional architecture of the nuclear pore complex. *Annu. Rev. Biophys.* 41:557–584.
8. Brohawn, S. G., J. R. Partridge, ..., T. U. Schwartz. 2009. The nuclear pore complex has entered the atomic age. *Structure*. 17:1156–1168.
9. Labokha, A. A., S. Gradmann, ..., D. Görlich. 2013. Systematic analysis of barrier-forming FG hydrogels from *Xenopus* nuclear pore complexes. *EMBO J.* 32:204–218.
10. Hülsmann, B. B., A. A. Labokha, and D. Görlich. 2012. The permeability of reconstituted nuclear pores provides direct evidence for the selective phase model. *Cell*. 150:738–751.
11. Strawn, L. A., T. Shen, ..., S. R. Wentz. 2004. Minimal nuclear pore complexes define FG repeat domains essential for transport. *Nat. Cell Biol.* 6:197–206.
12. Rexach, M., and G. Blobel. 1995. Protein import into nuclei: association and dissociation reactions involving transport substrate, transport factors, and nucleoporins. *Cell*. 83:683–692.

13. Dekker, C. 2007. Solid-state nanopores. *Nat. Nanotechnol.* 2:209–215.
14. Jovanovic-Taliman, T., J. Tetenbaum-Novatt, ..., B. T. Chait. 2009. Artificial nanopores that mimic the transport selectivity of the nuclear pore complex. *Nature.* 457:1023–1027.
15. Kowalczyk, S. W., L. Kapinos, ..., C. Dekker. 2011. Single-molecule transport across an individual biomimetic nuclear pore complex. *Nat. Nanotechnol.* 6:433–438.
16. Branton, D., D. W. Deamer, ..., J. A. Schloss. 2008. The potential and challenges of nanopore sequencing. *Nat. Biotechnol.* 26:1146–1153.
17. Miles, B. N., A. P. Ivanov, ..., J. B. Edel. 2013. Single molecule sensing with solid-state nanopores: novel materials, methods, and applications. *Chem. Soc. Rev.* 42:15–28.
18. Ivanov, A. P., E. Instuli, ..., J. B. Edel. 2011. DNA tunneling detector embedded in a nanopore. *Nano Lett.* 11:279–285.
19. Han, J., J. Fu, and R. B. Schoch. 2008. Molecular sieving using nano-filters: past, present and future. *Lab Chip.* 8:23–33.
20. Losic, D., and S. Simovic. 2009. Self-ordered nanopore and nanotube platforms for drug delivery applications. *Expert Opin. Drug Deliv.* 6:1363–1381.
21. Wanunu, M., and A. Meller. 2007. Chemically modified solid-state nanopores. *Nano Lett.* 7:1580–1585.
22. Wei, R., V. Gatterdam, ..., U. Rant. 2012. Stochastic sensing of proteins with receptor-modified solid-state nanopores. *Nat. Nanotechnol.* 7:257–263.
23. Peleg, O., M. Tagliazucchi, ..., I. Szleifer. 2011. Morphology control of hairy nanopores. *ACS Nano.* 5:4737–4747.
24. Moussavi-Baygi, R., Y. Jamali, ..., M. R. K. Mofrad. 2011. Biophysical coarse-grained modeling provides insights into transport through the nuclear pore complex. *Biophys. J.* 100:1410–1419.
25. Mincer, J. S., and S. M. Simon. 2011. Simulations of nuclear pore transport yield mechanistic insights and quantitative predictions. *Proc. Natl. Acad. Sci. USA.* 108:E351–E358.
26. Egorov, S. A., A. Milchev, ..., K. Binder. 2011. Structural properties of concave cylindrical brushes interacting with free chains. *Soft Matter.* 7:5669–5676.
27. Osmanovic, D., J. Bailey, ..., I. J. Ford. 2012. Bistable collective behavior of polymers tethered in a nanopore. *Phys. Rev. E Stat. Nonlin. Soft Matter Phys.* 85:061917.
28. Osmanović, D., A. Fassati, ..., B. W. Hoogenboom. 2013. Physical modelling of the nuclear pore complex. *Soft Matter.*
29. Paradise, A., M. K. Levin, ..., J. H. Carson. 2007. Significant proportions of nuclear transport proteins with reduced intracellular mobilities resolved by fluorescence correlation spectroscopy. *J. Mol. Biol.* 365: 50–65.
30. Schoch, R. L., L. E. Kapinos, and R. Y. H. Lim. 2012. Nuclear transport receptor binding avidity triggers a self-healing collapse transition in FG-nucleoporin molecular brushes. *Proc. Natl. Acad. Sci. USA.* 109: 16911–16916.
31. Ma, J., A. Goryaynov, ..., W. Yang. 2012. Self-regulated viscous channel in the nuclear pore complex. *Proc. Natl. Acad. Sci. USA.* 109:7326–7331.
32. Lowe, A. R., J. J. Siegel, ..., J. T. Liphardt. 2010. Selectivity mechanism of the nuclear pore complex characterized by single cargo tracking. *Nature.* 467:600–603.
33. Forwood, J. K., A. Lange, ..., B. Kobe. 2010. Quantitative structural analysis of importin- $\beta$  flexibility: paradigm for solenoid protein structures. *Structure.* 18:1171–1183.
34. Roth, R. 2010. Fundamental measure theory for hard-sphere mixtures: a review. *J. Phys. Condens. Matter.* 22:063102.
35. Jäkel, S., J.-M. Mingot, ..., D. Görlich. 2002. Importins fulfil a dual function as nuclear import receptors and cytoplasmic chaperones for exposed basic domains. *EMBO J.* 21:377–386.
36. Israelachvili, J. N. 2011. *Intermolecular and Surface Forces*, 3rd ed. Academic Press, New York.
37. Peleg, O., and R. Y. H. Lim. 2010. Converging on the function of intrinsically disordered nucleoporins in the nuclear pore complex. *Biol. Chem.* 391:719–730.
38. Wu, Y., G. Cheng, ..., G. D. Stucky. 2004. Composite mesostructures by nano-confinement. *Nat. Mater.* 3:816–822.
39. Lim, R. Y. H., B. Fahrenkrog, ..., U. Aebi. 2007. Nanomechanical basis of selective gating by the nuclear pore complex. *Science.* 318:640–643.
40. Adam, S. A., R. S. Marr, and L. Gerace. 1990. Nuclear protein import in permeabilized mammalian cells requires soluble cytoplasmic factors. *J. Cell Biol.* 111:807–816.
41. Peters, R. 2005. Translocation through the nuclear pore complex: selectivity and speed by reduction-of-dimensionality. *Traffic.* 6:421–427.
42. Ribbeck, K., and D. Görlich. 2001. Kinetic analysis of translocation through nuclear pore complexes. *EMBO J.* 20:1320–1330.
43. Goryaynov, A., J. Ma, and W. Yang. 2012. Single-molecule studies of nucleocytoplasmic transport: from one dimension to three dimensions. *Integr Biol (Camb).* 4:10–21.
44. Yang, W., and S. M. Musser. 2006. Nuclear import time and transport efficiency depend on importin  $\beta$  concentration. *J. Cell Biol.* 174: 951–961.
45. Grünwald, D., and R. H. Singer. 2010. In vivo imaging of labelled endogenous  $\beta$ -actin mRNA during nucleocytoplasmic transport. *Nature.* 467:604–607.
46. Mor, A., S. Suliman, ..., Y. Shav-Tal. 2010. Dynamics of single mRNA nucleocytoplasmic transport and export through the nuclear pore in living cells. *Nat. Cell Biol.* 12:543–552.
47. Adams, R. L., and S. R. Wente. 2013. Uncovering nuclear pore complexity with innovation. *cell.* 152:1218–1221.
48. Tagliazucchi, M., O. Peleg, ..., I. Szleifer. 2013. Effect of charge, hydrophobicity, and sequence of nucleoporins on the translocation of model particles through the nuclear pore complex. *Proc. Natl. Acad. Sci. USA.* 110:3363–3368.